Systematic Investigation of the Coupling between One-Dimensional Edge States of a Topological Crystalline Insulator

Johannes Jung,[1] Artem Odobesko,[1,*] Robin Boshuis,[1] Andrzej Szczerbakow,[2]
Tomasz Story,[2,3] and Matthias Bode[1]

[1]*Physikalisches Institut, Experimentelle Physik II, Universität Würzburg, Am Hubland, 97074 Würzburg, Germany*
[2]*Institute of Physics, Polish Academy of Sciences, Aleja Lotników 32/46, 02-668 Warsaw, Poland*
[3]*International Research Centre MagTop, Institute of Physics, Polish Academy of Sciences,*
Aleja Lotnikow 32/46, 02-668 Warsaw, Poland

The interaction of spin-polarized one-dimensional (1D) topological edge modes localized along single-atomic steps of the topological crystalline insulator $Pb_{0.7}Sn_{0.3}Se(001)$ has been studied systematically by scanning tunneling spectroscopy. Our results reveal that the coupling of adjacent edge modes sets in at a step-to-step distance $d_{ss} \leq 25$ nm, resulting in a characteristic splitting of a single peak at the Dirac point in tunneling spectra. Whereas the energy splitting exponentially increases with decreasing d_{ss} for single-atomic steps running almost parallel, we find no splitting for single-atomic step edges under an angle of 90°. The results are discussed in terms of overlapping wave functions with p_x, p_y orbital character.

Introduction.—The discovery of two-dimensional (2D) topological insulators (TIs), such as HgTe/CdTe [1] or InAs/GaSb quantum wells [2], generated significant attention, especially due to the existence of edge states protected by time-reversal symmetry. The spin-momentum locking pertinent to these states mandates that charge carriers with a given spin can only propagate in a predetermined direction, thereby inhibiting disorder scattering and greatly reducing dissipation in electrical transport [3–7]. Further material classes with topologically protected band structures have been predicted and realized, such as topological crystalline insulators (TCI) [8–11] and Weyl semimetals [12–17]. However, although the ruggedness of the respective topological states is often praised as one of their main advantages, the reliable realization of one-dimensional (1D) topological conductance channels highly relevant for practical applications remains a challenge. Some systems with topological 1D states, like higher-order topological hinge states [18,19], or surface step edges of weak TIs [20] or TCIs [21], could be identified, but systematic studies which address the interaction of adjacent channels remain elusive. As a result, the question up to which density topological 1D channels may be packed without compromising the signal quality has not yet been answered.

In this context hybridization effects of topological states play a particularly important role. For example, the close proximity to the underlying substrate may lead to a significant interaction of topological edge states with substrate bulk states [22–24]. Calculations predict that—if tuned appropriately—these effects may even be utilized, such as in topological-insulator–ferromagnetic-metal

(TI–FM) heterostructures, where hybridization-induced interface states lead to a large spin-transfer torque [25]. Strong hybridization between the top and the bottom surfaces, however, can also result in band crossings resulting in a trivial TCI phase [26] or—for very thin films of three-dimensional TIs—to the complete quenching of the topological surface state [27].

In this contribution we systematically study the interactions of one-dimensional topological states which arise at odd-atomic step edges of (001)-terminated (Pb,Sn)Se single crystals. Whereas the rock salt structure compound PbSe is a trivial insulator, the order of p-derived cation and anion surface states bands is inverted for $Pb_{1-x}Sn_xSe$ at $x \gtrsim 0.2$, i.e., when substituting a sufficient fraction of Pb atoms with Sn [9,28]. Band inversion results in four Dirac cones per surface Brillouin zone (SBZ) centered in close proximity to the $\bar{X}$ and $\bar{Y}$ points which are protected by ⟨110⟩ mirror symmetry [29–32].

Clean (001) surfaces of $Pb_{1-x}Sn_xSe$ are typically created by cleaving bulk crystals. As first shown in Ref. [33], tunneling spectra of flat (Pb,Sn)Se (001) surfaces exhibit a V-shaped dip with two symmetrically arranged side peaks which were assigned to the Dirac point and two van Hove singularities caused by saddle points in the dispersion, respectively. However, the cleaving process unavoidably also results in a variety of steps of different height and shape. The electronic structure of double- or other even-atomic step edges is virtually identical to a flat terrace, see the Supplemental Material [34], note 1. In contrast, a 1D topological edge mode was observed at odd-atomic step edges, e.g., steps with a height of one or three atomic layers. This edge mode is characterized by a strong peak in

the LDOS at the Dirac energy, as reported in Ref. [21] and confirmed in Ref. [39]. As detailed in Ref. [40], adjacent extended (001) terraces of (Pb,Sn)Se must—due to the displacement by one atomic layer in a two-atomic unit cell—be described by Hamiltonians with chiral symmetry and an inverted order of states. The resulting surface states are divided into two classes with an even or odd number of layers. Therefore, odd-atomic step edges host a doubly degenerate flat band at the Dirac energy that is protected by the mirror plane symmetry of the film [40].

In this Letter we systematically investigate the interaction between closely adjacent 1D edge states of the (001) surface of the TCI (Pb,Sn)Se. Hybridization is observed for step-to-step distances $d_{ss} \lesssim 25$ nm, resulting in the splitting of the single peak in tunneling spectra at the Dirac point into a double peak. Our results reveal that the energetic splitting exponentially increases with decreasing d_{ss}. It is largely insensitive to the details of a particular configuration of step edges as long as the steps run approximately in parallel. In contrast, for single-atomic steps crossing at an almost perpendicular angle, we do not observe any splitting.

Methods.—Experiments have been performed in an ultrahigh vacuum system equipped with a cryogenic STM (operation temperature $T = 4.9$ K). $Pb_{0.7}Sn_{0.3}Se$ p-doped single crystals grown by the self-selecting vapor growth method [9,21] (see the Supplemental Material [34], note 2, for further information) have been cleaved in UHV at a base pressure $p < 10^{-10}$ mbar and immediately transferred into the STM. Tunneling conductance dI/dU maps and spectra were measured by lock-in technique with modulation voltage $U_{mod} = 2.5$ mV at a frequency $f = 790$ Hz.

Results.—Figure 1(a) shows a typical STM topography image of the cleaved (001) surface of the TCI $Pb_{0.7}Sn_{0.3}Se$. Numerous wedge-shaped atomically flat plateaus can be recognized. The line profile measured along the green line in Fig. 1(a), presented in Fig. 1(b), reveals that most step edges are about 3 Å high, corresponding to half of the two-atomic unit cell. Figure 1(c) shows typical dI/dU spectra measured on a flat terrace far away from any step edge (1), on a double-atomic step edge (2), and at two single-atomic step edges [points (3),(4)]. Spectrum (1) exhibits a minimum at the Dirac point $E_D = (125 \pm 5)$ meV and two shoulders (L^- and L^+), which are associated with the two saddle points in the dispersion [30,33]. Spectrum (2) taken on a double-step edge is virtually indistinguishable from (1), indicating the absence of any edge state at step edges equivalent to an even number of atomic layers. In agreement with our earlier publication [21], a pronounced peak at the Dirac energy indicative for the 1D edge state can only be found at odd-atomic step edges, such as spectrum (3) measured on a single-atomic step edge. However, we find that the spectra of single-atomic step edges at some locations deviate from this simple single-peak structure.
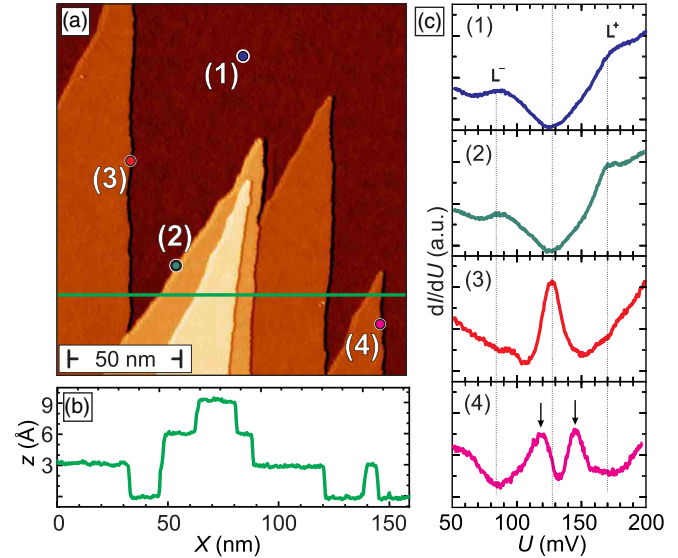

FIG. 1. (a) Topographic STM image of a cleaved $Pb_{0.7}Sn_{0.3}Se$ surface with a number of wedge-shaped terraces with a single- and double-atomic step edge height. (b) A line profile measured along the green line in (a). (c) Typical tunneling spectra measured on the plain terrace (1), double- (2) and single-atomic (3) step edges. Spectrum (4) with a characteristic double peak was obtained at a single-atomic step edge close to the pointed end of the wedge-shaped plateau. Stabilization parameters: $U_{set} = 200$ mV, $I_{set} = 0.2$ nA.

For example, the spectrum measured at (4) close to the termination point of an acute-angled wedge-shaped plateau reveals a pronounced double-peak feature in the vicinity of the Dirac point with a peak splitting of about 25 mV.

To understand the physical origin of this peak splitting we performed detailed spectroscopic investigations at numerous single-atomic step edge structures on a variety of topological $Pb_{0.7}Sn_{0.3}Se$ surfaces. Our results indicate that the peak splitting observed in Fig. 1(c) on the single-atomic step edge is not caused by the presence of kinks, defects, or random variations of the local doping level [41]. Instead, the data reveal that the splitting occurs when two single-atomic step edges are in close proximity. A particularly illustrative case is displayed in Fig. 2. The topographic STM image of Fig. 2(a) shows a wedge-shaped plateau bound by two single-atomic step edges which converge under an acute angle of $3.4° \pm 0.3°$. As a result, the step-to-step distance d_{ss} slowly decreases over a total length of about 500 nm from $d_{ss} > 30$ nm in the bottom part to almost zero at the apex of the wedge. Both steps have rough edges which clearly deviate from high symmetry directions. Nevertheless, the dI/dU map measured at a bias voltage corresponding to the Dirac point presented in Fig. 2(b) shows several unique features. First, in the bottom part of Fig. 2(b), where the two single-atomic step edges are far apart, an intense dI/dU signal can be recognized along the step edges, indicating the presence of the topological
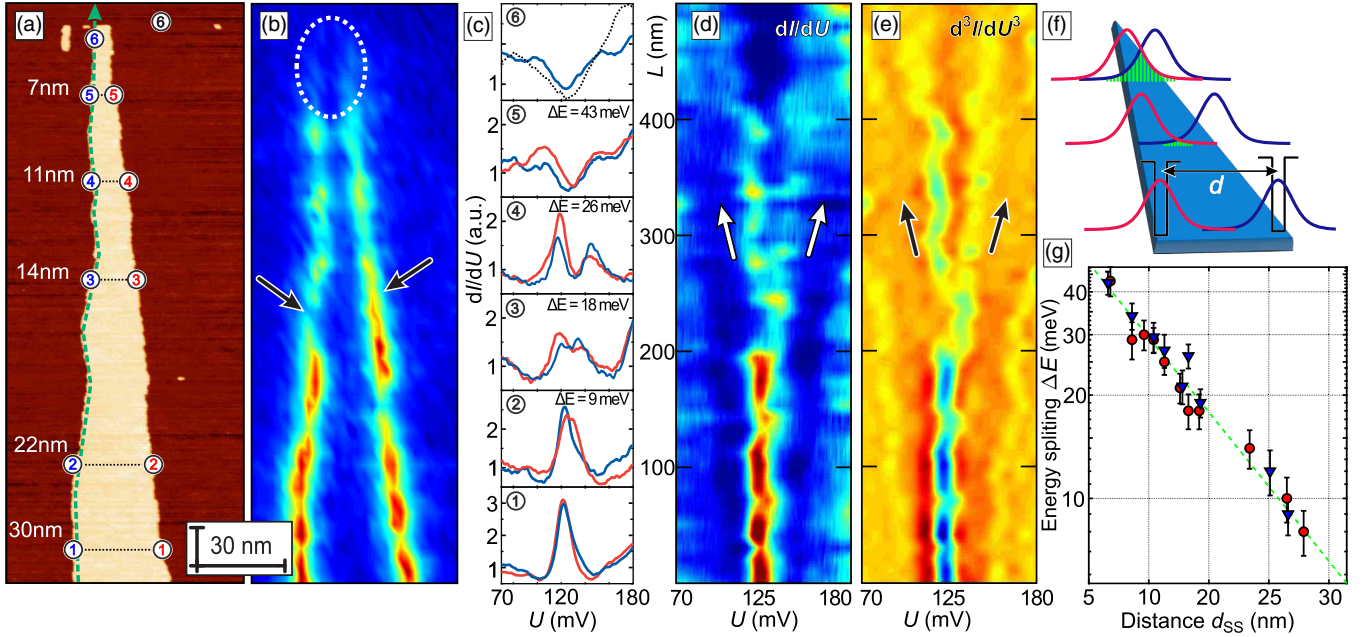
FIG. 2.   (a) Topographic STM image of a wedge-shaped plateau surrounded by single-atomic step edges. Note, that the x and y direction are scaled differently, i.e., the wedge shape is even more acute angled than it appears. (b) dI/dU map measured at the Dirac energy of the same region shown in (a). An enhanced intensity at the position of the step edges is clearly visible in the bottom part, indicating the presence of the topologically protected edge state. As the wedge-shaped plateau becomes more narrow, the intensity of the dI/dU signal measured at both step edges decreases (see region above arrows) and eventually vanishes close to the termination point (ellipse). (c) Tunneling spectra measured at the left (blue) and right (red) single-atomic step edge at various step-to-step distances indicated in (a). (d) Color-coded raw dI/dU spectra measured along the green hatched line in (a). (e) Numerically calculated second derivative (d^3I/dU^3) of (d). (f) Sketch of a model of two quantum wells localized along two converging single-atomic step edges. The wave functions extend beyond the walls and overlap. The overlap area (green) indicates the coupling strength and determines the energy splitting. (g) The peak energy splitting ΔE in dependence of step-to-step distance in semilogarithmic scale. Stabilization parameters: (a), (b) $U_{\mathrm{set}} = 125$ mV (a), $I_{\mathrm{set}} = 0.2$ nA.

edge state. Second, as d_{ss} falls below about 15 nm, indicated by two arrows in Fig. 2(b), the intensity of the dI/dU signal noticeably decreases. Third, close to the top of the wedge where $d_{\mathrm{ss}} \lesssim 7$ nm (marked by a hatched ellipse) it becomes essentially indistinguishable from the signal measured on the surrounding terraces.

This modification of the LDOS at the Dirac energy correlates with a systematic alteration of the local STS data. Some exemplary spectra measured at various step-to-step distances ranging from $d_{\mathrm{ss}} = 30$ down to $d_{\mathrm{ss}} = 7$ nm are shown in Fig. 2(c). In each case we present the spectra measured at the left and the right single-atomic step edge in blue and red, respectively. The tunneling spectra measured at $d_{\mathrm{ss}} = 30$ nm (curve ①) exhibit a single intense peak at the Dirac energy $E_D = 125$ meV which is fully consistent with the spectra measured at isolated step edges [21]. At $d_{\mathrm{ss}} = 22$ nm (curve ②) the peak height slightly decreases and a weak shoulder (blue curve) or subtle double humps (red curve) can be recognized. With d_{ss} reduced to 14 nm (curve ③) a clear splitting in two peaks becomes apparent, which amounts to $\Delta E \approx 18$ mV. The splitting further increases with decreasing step-to-step distance reaching $\Delta E \approx 26$ meV at $d_{\mathrm{ss}} = 11$ nm (curve ④). At $d_{\mathrm{ss}} = 7$ nm

the peak intensities have drastically dropped (curve ⑤), even though the splitting still appears to increase ($\Delta E \approx 43$ meV). Eventually, at even smaller d_{ss} the peaks become almost undistinguishable from the spectra of the terrace (curve ⑥ and dashed line, respectively).

Figure 2(d) represents the complete dataset of color-coded raw dI/dU spectra measured along the green hatched line in Fig. 2(a). This line section follows the contour of the left single-atomic step edge for about 500 nm from the bottom of Fig. 2(a) ($L = 0$) all the way to its termination point at the upper part of the wedge-shaped plateau. For better contrast the numerically calculated second derivative of the dI/dU signal, i.e., d^3I/dU^3, is presented in Fig. 2(e). At 0 nm $\leq L \leq 200$ nm the data confirm the existence of a single peak at the Dirac energy $E_D = eU \approx 125$ meV. Local fluctuations by about ± 5 mV are probably caused by statistical variations of the substitutional dopant concentration [41,42]. As indicated by arrows in Fig. 2(d) and 2(e), for $L \geq 250$ nm the single peak which is known to represent the topological edge state of (Pb,Sn) Se [21] splits into two diverging branches. The data presented in Fig. 2(e) reveal the peak splitting increases with decreasing step-to-step distance up to $L \leq 400$ nm

where $\Delta E \approx 28$ meV at $d_{ss} \approx 10$ nm. Above this line both peaks experience significant peak broadening and strongly decrease in intensity, possibly due to the onset of attenuation. As presented in detail in the Supplemental Material [34], note 3, the results obtained on the right step edge are fully consistent with the results presented for the left step edge in Fig. 2. Furthermore, these main findings are independent of the specific type and shape of the step edges. For example, results presented in the Supplemental Material [34], notes 4 and 5, confirm that the peak splitting also exists for wedge-shaped vacancy islands and nearby parallel steps, respectively.

Discussion.—Similar observations of a coupling-dependent energy splitting have been made for zero-dimensional quantum dots [43] and two-dimensional layered van der Waals heterostructures [44]. In the latter case the opening of band gaps was particularly prominent for out-of-plane–oriented MoS_2 orbitals which strongly overlap with graphene π bands [44]. In fact, periodic boundary calculations presented in Fig. 6 of Ref. [40] suggest that the topological 1D edge state of (Pb,Sn)Se remains largely unaffected for terrace width $d_{ss} \geq 86$ nm, in reasonable agreement with our experimental data, cf. Fig. 2. Similar to the tight binding calculations presented in Ref. [21], a weak splitting may be visible for $d_{ss} \geq 43$ nm [40]. For narrower terraces, however, a collapse of the double Dirac cone into a single cone with a crossing at the $\bar{X}$ point was predicted [40], in clear disagreement with our results that show the persistence of a split peak well below $d_{ss} \leq 10$ nm, cf. Fig. 2.

To simulate the observed behavior, we assume that the formation of the edge state results in an increased local density of states, crammed in a narrow region around the step edge. This regions of accumulated charge are—in a first-order approach—modeled by narrow identical quantum wells with a width ~ 1 nm perpendicular to the step edge and much larger along the step edge, determined as the intra-row coherence length. For a perfect step edge the topological edge mode would be completely delocalized along the step edge. The fact that the energy splitting observed at different points along the step edge depends on the step-to-step distance suggests that we do not deal with a single, infinitely extended quantum state, but with electron wave functions which are localized to a certain extent due to their finite coherence length, potentially induced by disorder. Two quantum wells are separated by a distance d and affect the edge state; see Fig. 2(f). The well depth is assumed to ~ 100 meV, corresponding to the bulk band gap of the $Pb_{0.7}Sn_{0.3}Se$ [45]. As shown in detail in the Supplemental Material [34], note 6, both quantum wells host wave functions which extend beyond their respective boundaries and decay exponentially with $\exp(-(x/\xi))$ outside the well, with the decay length ξ.

When the wave functions overlap at low d, see green area in Fig. 2(f), the exponentially decaying tails of the wave functions couple, resulting in an energy splitting ΔE.

Indeed, a plot of ΔE values extracted from Fig. 2(e) versus d_{ss} confirms the expected exponential dependence, see Fig 2(g). The decay length of the 1D edge mode perpendicular to the step direction is determined to $\xi = (10 \pm 1)$ nm. By taking $\hbar \delta k \propto \hbar / 2\xi$ and $\delta E \approx 10$ meV as the width of the single peak in spectrum ① of Fig. 2(c), we estimate the group velocity to $v_{gr} \approx \delta E / \hbar \delta k \approx 3 \times 10^5$ m/s, in good agreement with earlier band dispersion measurements [31,46].

Orthogonal step edges.—Our investigations of wedge-shaped islands like those presented in Figs. 1 and 2 suggest that wedge angles are always $\lesssim 30°$. In contrast, much larger adjacent angles were regularly observed at points where two single-atomic steps intersect. For example, the STM data of Fig. 3(a) show two steps oriented along the planar high-symmetry $\langle 100 \rangle$ directions intersecting under an angle of $\approx 90°$. Again, we find a strongly enhanced dI/dU signal at the Dirac energy at the location of odd-atomic step edges and a strong reduction at the step crossing point, Fig. 3(b). In contrast to the situation observed for wedge-shaped step edges in Fig. 2, however, the tunneling spectra measured along the white arrow in panel Fig. 3(a) show no hints for any peak splitting, see Figs. 3(c) and 3(d) for raw spectra and d^3I/dU^3, respectively. The full dataset is presented in the Supplemental Material [34], note 7.

The results presented in Figs. 2, 3 and Ref. [34] show that the topological edge state characteristic for odd-atomic step edges of the (Pb,Sn)Se (001) surface splits for adjacent steps ($d_{ss} \lesssim 25$ nm) running in parallel or under an acute angle. In contrast, for step edges crossing perpendicularly
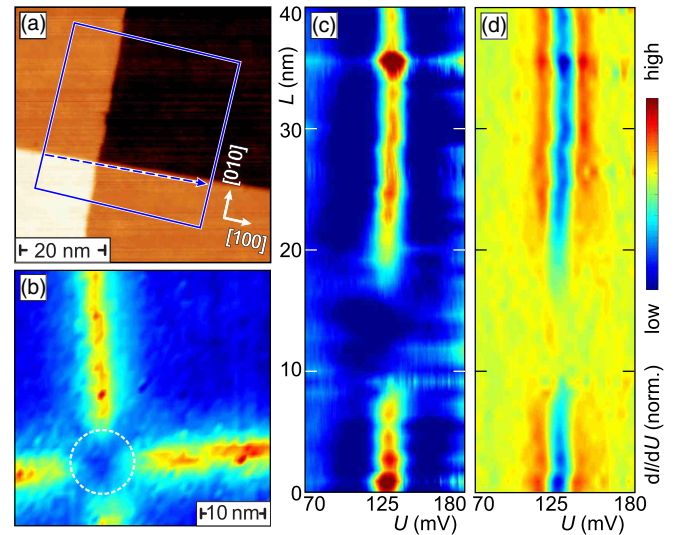

FIG. 3. (a) Topography and (b) dI/dU map measured at the Dirac point ($U_{set} = 120$ mV)) of two intersecting at 90° single-step edges, both running along the sample's high symmetry directions. (c) Color-coded raw dI/dU spectra measured along step-edge running in [100] marked with the hatched line in (a);. (d) Second derivative (d^3I/dU^3) of the same signal in (c). Stabilization parameters: $U_{set} = 120$ mV, $I_{set} = 0.2$ nA.

no such peak splitting is observed. This latter behavior hints at wave functions which are orthogonal such that the solution of the Schrödinger equation becomes $\int \Phi_n^* \Phi_m dV = \delta_{n,m}$, where the indices n, m stand for quantum numbers and $\delta_{n,m}$ is the Kronecker symbol. Obvious choices for this quantum number might be the spin or the orbital moment of the edge state. We are convinced that we can exclude the spin since results obtained within a tight binding [21] or envelope function model [40] indicate an out-of-plane or vanishing spin polarization of the edge state, respectively, both insufficient to explain the absence of a peak splitting for orthogonal edge states. In contrast, the contribution of a Se p_x and p_y orbital momentum to the Dirac points at $\bar{X}$ and $\bar{Y}$ has been described theoretically [40,46,47] and nicely corresponds with our experimental findings. In order to test this interpretation we investigated intersections of two single-atomic steps at angles below but close to 90°. Indeed, for single-atomic steps that cross under a 60° angle we observe a very weak but detectable splitting, see the Supplemental Material [34], note 8. It is not clear, however, if the spin-orbit coupling in (Pb,Sn)Se plays any role. This question remains to be clarified by future theoretical investigations.

Conclusion.—In conclusion, we have studied the interaction of adjacent 1D spin-polarized edge states which are localized at single-atomic step edges of the TCI $Pb_{0.7}Sn_{0.3}Se(001)$. Coupling at a step-to-step distance $d_{ss} \lesssim 25$ nm leads to the energy splitting of the single peak in LDOS at the Dirac point into two. The energy splitting increases exponentially with decreasing d_{ss} and reveals the localized character of the topological edge mode, instead of the single quantum state. At a very small separation ($d_{ss} \lesssim 10$ nm) the two peaks strongly decrease in intensity. No peak splitting is found for perpendicular single-atomic step edges, suggesting an important role of the Se p_x and p_y orbital momentum of the edge state.

Note added in the proof.—After acceptance of this work the authors of Ref. [40] informed us that their model only results in a quenching of the topological edge state for periodically arranged step edges. In contrast, in an effective model, the bands localized on two nearby steps split in energy and the splitting increases with decreasing the distance between the steps if there are just two steps in close proximity, surrounded by a flat surface, in rough quantitative agreement with the results obtained in this paper.

---

*Corresponding author.
artem.odobesko@physik.uni-wuerzburg.de

[1] M. König, S. Wiedmann, C. Brüne, A. Roth, H. Buhmann, L. W. Molenkamp, X.-L. Qi, and S.-C. Zhang, Quantum spin hall insulator state in HgTe quantum wells, Science **318**, 766 (2007).

[2] I. Knez, R.-R. Du, and G. Sullivan, Evidence for Helical Edge Modes in Inverted InAs/GaSb Quantum Wells, Phys. Rev. Lett. **107**, 136603 (2011).

[3] S. Bauer and C. A. Bobisch, Nanoscale electron transport at the surface of a topological insulator, Nat. Commun. **7**, 11381 (2016).

[4] Y. Hou, R. Wang, R. Xiao, L. McClintock, H. C. Travaglini, J. P. Francia, H. Fetsch, O. Erten, S. Y. Savrasov, B. Wang, A. Rossi, I. Vishik, E. Rotenberg, and D. Yu, Millimetre-long transport of photogenerated carriers in topological insulators, Nat. Commun. **10**, 5723 (2019).

[5] P. Liu, J. R. Williams, and J. J. Cha, Topological nanomaterials, Nat. Rev. Mater. **4**, 479 (2019).

[6] L. Plucinski, Band structure engineering in 3D topological insulators, J. Phys. Condens. Matter **31**, 183001 (2019).

[7] C.-W. Liu, Z. Wang, R. L. J. Qiu, and X. P. A. Gao, Development of topological insulator and topological crystalline insulator nanostructures, Nanotechnology **31**, 192001 (2020).

[8] L. Fu, Topological Crystalline Insulators, Phys. Rev. Lett. **106**, 106802 (2011).

[9] P. Dziawa, B. J. Kowalski, K. Dybko, R. Buczko, A. Szczerbakow, M. Szot, E. Lusakowska, T. Balasubramanian, B. M. Wojek, M. H. Berntsen, O. Tjernberg, and T. Story, Topological crystalline insulator states in $Pb_{1-x}Sn_xSe$, Nat. Mater. **11**, 1023 (2012).

[10] S.-Y. Xu *et al.*, Observation of a topological crystalline insulator phase and topological phase transition in $Pb_{1-x}Sn_xTe$, Nat. Commun. **3**, 1192 (2012).

[11] Y. Tanaka, Z. Ren, T. Sato, K. Nakayama, S. Souma, T. Takahashi, K. Segawa, and Y. Ando, Experimental realization of a topological crystalline insulator in SnTe, Nat. Phys. **8**, 800 (2012).

[12] H. Weng, C. Fang, Z. Fang, B. A. Bernevig, and X. Dai, Weyl Semimetal Phase in Noncentrosymmetric Transition-Metal Monophosphides, Phys. Rev. X **5**, 011029 (2015).

[13] S.-Y. Xu *et al.*, Discovery of a Weyl fermion semimetal and topological Fermi arcs, Science **349**, 613 (2015).

[14] B. Q. Lv, H. M. Weng, B. B. Fu, X. P. Wang, H. Miao, J. Ma, P. Richard, X. C. Huang, L. X. Zhao, G. F. Chen, Z. Fang, X. Dai, T. Qian, and H. Ding, Experimental Discovery of Weyl semimetal TaAs, Phys. Rev. X **5**, 031013 (2015).

[15] L. X. Yang, Z. K. Liu, Y. Sun, H. Peng, H. F. Yang, T. Zhang, B. Zhou, Y. Zhang, Y. F. Guo, M. Rahn, D. Prabhakaran, Z. Hussain, S. K. Mo, C. Felser, B. Yan,

and Y. L. Chen, Weyl semimetal phase in the non-centrosymmetric compound TaAs, Nat. Phys. **11,** 728 (2015).

[16] B. Q. Lv, N. Xu, H. M. Weng, J. Z. Ma, P. Richard, X. C. Huang, L. X. Zhao, G. F. Chen, C. E. Matt, F. Bisti, V. N. Strocov, J. Mesot, Z. Fang, X. Dai, T. Qian, M. Shi, and H. Ding, Observation of Weyl nodes in TaAs, Nat. Phys. **11,** 724 (2015).

[17] P. Sessi, Y. Sun, T. Bathon, F. Glott, Z. Li, H. Chen, L. Guo, X. Chen, M. Schmidt, C. Felser, B. Yan, and M. Bode, Impurity screening and stability of Fermi arcs against Coulomb and magnetic scattering in a Weyl monopnictide, Phys. Rev. B **95,** 035114 (2017).

[18] I. K. Drozdov, A. Alexandradinata, S. Jeon, S. Nadj-Perge, H. Ji, R. J. Cava, A. B. Bernevig, and A. Yazdani, One-dimensional topological edge states of bismuth bilayers, Nat. Phys. **10,** 664 (2014).

[19] F. Schindler, Z. Wang, M. G. Vergniory, A. M. Cook, A. Murani, S. Sengupta, A. Y. Kasumov, R. Deblock, S. Jeon, I. Drozdov, H. Bouchiat, S. Guéron, A. Yazdani, B. A. Bernevig, and T. Neupert, Higher-order topology in bismuth, Nat. Phys. **14,** 918 (2018).

[20] C. Pauly, B. Rasche, K. Koepernik, M. Liebmann, M. Pratzer, M. Richter, J. Kellner, M. Eschbach, B. Kaufmann, L. Plucinski, C. M. Schneider, M. Ruck, J. van den Brink, and M. Morgenstern, Subnanometre-wide electron channels protected by topology, Nat. Phys. **11,** 338 (2015).

[21] P. Sessi, D. Di Sante, A. Szczerbakow, F. Glott, S. Wilfert, H. Schmidt, T. Bathon, P. Dziawa, M. Greiter, T. Neupert, G. Sangiovanni, T. Story, R. Thomale, and M. Bode, Robust spin-polarized midgap states at step edges of topological crystalline insulators, Science **354,** 1269 (2016).

[22] T. Hirahara, G. Bihlmayer, Y. Sakamoto, M. Yamada, H. Miyazaki, S. I. Kimura, S. Blügel, and S. Hasegawa, Interfacing 2D and 3D Topological Insulators: Bi(111) Bilayer on Bi_2Te_3, Phys. Rev. Lett. **107,** 166801 (2011).

[23] F. Yang, L. Miao, Z. F. Wang, M.-Y. Yao, F. Zhu, Y. R. Song, M.-X. Wang, J.-P. Xu, A. V. Fedorov, Z. Sun, G. B. Zhang, C. Liu, F. Liu, D. Qian, C. L. Gao, and J.-F. Jia, Spatial and Energy Distribution of Topological Edge States in Single Bi(111) Bilayer, Phys. Rev. Lett. **109,** 016801 (2012).

[24] S. H. Kim, K.-H. Jin, J. Park, J. S. Kim, S.-H. Jhi, T.-H. Kim, and H. W. Yeom, Edge and interfacial states in a two-dimensional topological insulator: Bi(111) bilayer on Bi_2Te_2Se, Phys. Rev. B **89,** 155436 (2014).

[25] Y.-T. Hsu, K. Park, and E.-A. Kim, Hybridization-induced interface states in a topological-insulator–ferromagnetic-metal heterostructure, Phys. Rev. B **96,** 235433 (2017).

[26] J. Liu, T. H. Hsieh, P. Wei, W. Duan, J. Moodera, and L. Fu, Spin-filtered edge states with an electrically tunable gap in a two-dimensional topological crystalline insulator, Nat. Mater. **13,** 178 (2014).

[27] Y. Zhang, K. He, C.-Z. Chang, C.-L. Song, L.-L. Wang, X. Chen, J.-F. Jia, Z. Fang, X. Dai, W.-Y. Shan, S.-Q. Shen, Q. Niu, X.-L. Qi, S.-C. Zhang, X.-C. Ma, and Q.-K. Xue, Crossover of the three-dimensional topological insulator Bi_2Se_3 to the two-dimensional limit, Nat. Phys. **6,** 584 (2010).

[28] B. M. Wojek, P. Dziawa, B. J. Kowalski, A. Szczerbakow, A. M. Black-Schaffer, M. H. Berntsen, T. Balasubramanian,

T. Story, and O. Tjernberg, Band inversion and the topological phase transition in (Pb,Sn)Se, Phys. Rev. B **90,** 161202(R) (2014).

[29] T. H. Hsieh, H. Lin, J. Liu, W. Duan, A. Bansil, and L. Fu, Topological crystalline insulators in the SnTe material class, Nat. Commun. **3,** 982 (2012).

[30] J. Liu, W. Duan, and L. Fu, Two types of surface states in topological crystalline insulators, Phys. Rev. B **88,** 241303 (R) (2013).

[31] Y. J. Wang, W.-F. Tsai, H. Lin, S.-Y. Xu, M. Neupane, M. Z. Hasan, and A. Bansil, Nontrivial spin texture of the coaxial Dirac cones on the surface of topological crystalline insulator SnTe, Phys. Rev. B **87,** 235317 (2013).

[32] S. Safaei, P. Kacman, and R. Buczko, Topological crystal-line insulator (Pb,Sn)Te: Surface states and their spin polarization, Phys. Rev. B **88,** 045305 (2013).

[33] Y. Okada, M. Serbyn, H. Lin, D. Walkup, W. Zhou, C. Dhital, M. Neupane, S. Xu, Y. J. Wang, R. Sankar, F. Chou, A. Bansil, M. Z. Hasan, S. D. Wilson, L. Fu, and V. Madhavan, Observation of Dirac node formation and mass acquisition in a topological crystalline insulator, Science **341,** 1496 (2013).

[34] See Supplemental Material at http://link.aps.org/supplemental/10.1103/PhysRevLett.126.236402 for detailed information regarding the electronic structure of odd- and even-atomic step edges, details regarding crystal synthesis and characterization, further data obtained on wedge-shaped islands and depressions, the asymmetric energy splitting observed for two parallel single-atomic steps, our model of two interacting 1D edge modes, single-atomic steps crossing under angles of about 60° and 90°, and fluctuations of the Dirac energy, which includes Refs. [35–38].

[35] I. Zeljkovic, Y. Okada, M. Serbyn, R. Sankar, D. Walkup, W. Zhou, J. Liu, G. Chang, Y. J. Wang, M. Z. Hasan, F. Chou, H. Lin, A. Bansil, L. Fu, and V. Madhavan, Dirac mass generation from crystal symmetry breaking on the surfaces of topological crystalline insulators, Nat. Mater. **14,** 318 (2015).

[36] A. Szczerbakow and H. Berger, Investigation of the composition of vapour-grown $Pb_{(1-x)}Sn_xSe$ crystals ($x \leq 0.4$) by means of lattice parameter measurements, J. Cryst. Growth **139,** 172 (1994).

[37] A. Szczerbakow and K. Durose, Self-selecting vapour growth of bulk crystals—principles and applicability, Prog. Cryst. Growth Charact. Mater. **51,** 81 (2005).

[38] P. Hofmann, *Solid State Physics: An Introduction* (John Wiley & Sons, New York, 2015).

[39] D. Iaia, C.-Y. Wang, Y. Maximenko, D. Walkup, R. Sankar, F. Chou, Y.-M. Lu, and V. Madhavan, Topological nature of step-edge states on the surface of the topological crystalline insulator $Pb_{0.7}Sn_{0.3}Se$, Phys. Rev. B **99,** 155116 (2019).

[40] R. Rechciński and R. Buczko, Topological states on uneven (Pb,Sn)Se (001) surfaces, Phys. Rev. B **98,** 245302 (2018).

[41] H. Beidenkopf, P. Roushan, J. Seo, L. Gorman, I. Drozdov, Y. S. Hor, R. J. Cava, and A. Yazdani, Spatial fluctuations of helical Dirac fermions on the surface of topological insula-tors, Nat. Phys. **7,** 939 (2011).

[42] O. Storz, A. Cortijo, S. Wilfert, K. A. Kokh, O. E. Tereshchenko, M. A. H. Vozmediano, M. Bode, F. Guinea,

and P. Sessi, Mapping the effect of defect-induced strain disorder on the Dirac states of topological insulators, Phys. Rev. B **94**, 121301(R) (2016).

[43] M. Nilsson, F. V. Boström, S. Lehmann, K. A. Dick, M. Leijnse, and C. Thelander, Tuning The Two-Electron Hybridization and Spin States in Parallel-Coupled InAs Quantum Dots, Phys. Rev. Lett. **121**, 156802 (2018).

[44] H. C. Diaz, J. Avila, C. Chen, R. Addou, M. C. Asensio, and M. Batzill, Direct observation of interlayer hybridization and Dirac relativistic carriers in graphene/MoS_2 van der Waals heterostructures, Nano Lett. **15**, 1135 (2015).

[45] We would like to note that we cannot exclude that similar or even better results can be obtained by more elaborate models, where the electrostatic interaction becomes less relevant and is instead replaced by a behavior governed by spatially varying topological indices.

[46] I. Zeljkovic, Y. Okada, C.-Y. Huang, R. Sankar, D. Walkup, W. Zhou, M. Serbyn, F. Chou, W.-F. Tsai, H. Lin, A. Bansil, L. Fu, M. Z. Hasan, and V. Madhavan, Mapping the unconventional orbital texture in topological crystalline insulators, Nat. Phys. **10**, 572 (2014).

[47] B. M. Wojek, R. Buczko, S. Safaei, P. Dziawa, B. J. Kowalski, M. H. Berntsen, T. Balasubramanian, M. Leandersson, A. Szczerbakow, P. Kacman, T. Story, and O. Tjernberg, Spin-polarized (001) surface states of the topological crystalline insulator $Pb_{0.73}Sn_{0.27}Se$, Phys. Rev. B **87**, 115106 (2013).